Sci. Bull.
DOI 10.1007/s11434-015-0805-0

www.scibull.com
www.springer.com/scp

Article

Chemistry

Effect of reduction–oxidation treatment on structure and catalytic properties of ordered mesoporous Cu–Mg–Al composite oxides

Jingting Lu · Yan Zhang · Chengli Jiao · Suresh Kumar Megarajan · Dong Gu · Guocheng Yang · Heqing Jiang · Chunjiang Jia · Ferdi Schüth

Received: 11 March 2015 / Accepted: 4 April 2015

Abstract Ordered mesoporous Cu–Mg–Al composite oxides were synthesized via the one-pot evaporation-induced self-assembly strategy. Using this method, copper was first homogeneously incorporated into the ordered mesoporous spinel matrix. After H_2 reduction treatment, according to X-ray diffraction (XRD) and transmission electron microscopy (TEM) results, copper existed as metallic nanoparticles with the size of 6–10 nm that well decorated the parent mesoporous skeleton. The metallic nanoparticles were then re-oxidized to copper oxide when exposed to air or during CO oxidation reaction at low temperatures. Thus, copper migrated from bulk spinel phase to the surface after the reduction–oxidation treatment. Moreover, the copper on the surface was re-incorporated into the bulk spinel phase by further thermal treatment at much higher temperature in the presence of air. The correlation between the state of copper in the mesoporous composite oxides and the catalytic performance toward CO oxidation was studied. It was found that copper existed as oxide nanoparticles on the surface of mesoporous Mg–Al skeleton is much more active than that existed as lattice Cu ions in spinel phase.

Keywords Cu–Mg–Al oxides · Evaporation-induced self-assembly · Mesoporous materials · Migration · CO oxidation

1 Introduction

Mixed metal oxides have attracted increasing interest in the past decades because of their potential application in sensors, separation, and catalysis [1–4]. Former experimental and theoretical studies have indicated that the state of active component in the composite catalysts strongly influences the catalytic performance. For example, Zhang's group [5, 6] compared the noble metal substituted and supported hexaaluminate catalysts for high-concentration N_2O decomposition. They concluded that the framework noble metals (Ir and/or Ru) incorporated into the hexaaluminate lattice were more active than the large Ir and/or Ru oxide species agglomerated outside the hexaaluminate structure. Burch [7, 8] observed that fully oxidized PdO on the surface of Al_2O_3 was the optimum state for complete methane oxidation compared to the highly dispersed metallic Pd supported by Al_2O_3. To obtain a better catalytic performance, it is obviously necessary to finely adjust the state of active component in the composite catalysts.

In addition, the catalytic performance and behaviors are closely related to the structure characteristics of the

Jingting Lu and Yan Zhang contributed equally to this work.

J. Lu · G. Yang (✉)
School of Chemistry and Life Science, Changchun University of Technology, Changchun 130012, China
e-mail: ychenguo@yahoo.com

J. Lu · Y. Zhang · C. Jiao · Suresh KumarMegarajan · H. Jiang (✉)
Key Laboratory of Biobased Materials, Qingdao Institute of Bioenergy and Bioprocess Technology, Chinese Academy of Sciences, Qingdao 266101, China
e-mail: jianghq@qibebt.ac.cn

D. Gu · F. Schüth
Max-Planck-Institut für Kohlenforschung, Kaiser-Wilhelm-Platz 1, 45470 Mülheim an der Ruhr, Germany

C. Jia
Key Laboratory for Colloid and Interface Chemistry, Key Laboratory of Special Aggregated Materials, School of Chemistry and Chemical Engineering, Shandong University, Jinan 250100, China

Published online: 09 May 2015

materials, such as surface area, pore width, and porous structure. Ordered mesoporous alumina, like other mesoporous materials [9, 10], has been considered as promising support or catalyst for various catalytic applications, because of its large surface area, narrow pore size distribution, highly uniform channels, and tunable pore sizes over a considerably wide range [11–14]. The development of strategies for synthesizing these mesoporous materials, such as traditional precipitation [15], nanocasting [16], sol–gel process [17], and cation–anion double hydrolysis [18], was therefore widely stimulated during the last decades. Among various synthesis routes, the solvent evaporation-induced self-assembly (EISA) strategy [19] attracted increasing attentions due to its simple, reliable, and reproducible properties, which allows the fine-tuning of structure properties of the materials. Later, this method was further extended to synthesize mesoporous alumina-supported metal oxides (NiO, Cr_2O_3, CeO_2, etc.) [20–23], and the high-quality mesoporous structure with strong metal–support interactions and homogeneous distribution of active component was observed [24, 25].

Here, we extend this approach to facilely synthesize the Cu–Mg–Al oxides. In this ternary system, copper was first homogeneously incorporated into the mesoporous spinel framework due to the special advantages of the one-pot EISA synthesis method. By taking a reduction–oxidation treatment on mesoporous Cu–Mg–Al oxides, copper migrated from bulk spinel phase to the surface and finally existed as small particles that well decorated mesoporous Mg–Al spinel network. The structure property and aggregation state of Cu in the mesoporous composite oxides were studied in this work, which was further correlated with the catalytic performance toward CO oxidation.

2 Experimental

2.1 Catalyst preparation

The mesoporous Cu–Mg–Al composite oxide with 5 % molar fraction of copper and 10 % molar fraction of magnesium was prepared via the evaporation-induced self-assembly route using Pluronic P123 as a structure directing agent as reported [19, 20]. Typically, Pluronic P123 ($EO_{20}PO_{70}EO_{20}$, 1.0 g) was dissolved in ethanol (20 mL) with small vortex stirring at room temperature for 4 h. Then 67 wt% nitric acid (1.6 mL) and the appropriate quantity of copper (II) nitrate trihydrate (99 %–102 %), magnesium (II) nitrate hexahydrate (≥99 %), and aluminum isopropoxide (98 %) were added into the above solution with vigorous stirring. The beaker containing the mixture was covered with PE film and vigorously stirred at room temperature for about 12 h and then followed by a solvent evaporation at 60 °C for 2 d in a drying oven. The obtained solid was then calcined by slowing increasing temperature (1 °C min^{-1} ramping rate) from room temperature to 400 °C and holding for 4 h under flowing air to receive the Cu–Mg–Al-400 for simplicity. The final Cu–Mg–Al spinel catalyst was obtained by further treating the above sample at 800 °C for 4 h (heating rate 3 °C min^{-1}) and was denoted as Cu–Mg–Al–SP (SP: SPinel) in the following description. After the sample Cu–Mg–Al–SP was further treated under 5 vol% H_2 (N_2 as the balance) at 650 °C for 4 h, copper was reduced and existed as nanoparticles on the surface of mesoporous Mg–Al spinel, which was denoted as Cu–Mg–Al–SF (SF: SurFace). The sample Cu–Mg–Al–SF–SP was obtained by further treating the spent Cu–Mg–Al–SF using reaction gas (O_2/CO/N_2 = 1:1:98) at 650 °C for 1 h.

The mesoporous Mg–Al composite oxides were also prepared by the above EISA strategy without copper (II) nitrate trihydrate in the starting materials. The final fabricated samples were abbreviated as Mg–Al-400 and Mg–Al–SP, which represent the above composite calcined at 400 and 800 °C, respectively.

2.2 Catalyst characterization

Powder X-ray diffraction (XRD) patterns were collected on a Bruker D8 ADVANCE diffractometer with Cu Kα radiation from 0.6° to 4.5° (small angle) and 10° to 80° (wide angle) at room temperature. Transmission electron microscopy (TEM) was taken on a Hitachi H-7650 microscope under a working voltage of 100 kV. Nitrogen adsorption and desorption isotherms were recorded on a NOVA 4200e instrument at −196 °C. Prior to the measurements, the samples were degassed under vacuum at 150 °C for 6 h. The surface area was calculated using the Brunauer–Emmett–Teller (BET) method. Temperature-programmed reduction (TPR) of H_2 was performed on a homemade apparatus, using a gas mixture of 4.5 vol% H_2 in N_2 at a flow of 30 mL min^{-1}. Thirty milligrams of sample was used for each measurement. The temperature was raised from room temperature to 600 °C at a heating rate of 10 °C min^{-1}. A thermal conductivity detector (TCD) was used on line for monitoring the H_2 consumption.

2.3 Activity test

The catalytic measurements on CO oxidation were carried out in a fixed-bed corundum reactor. Five hundred milligrams of catalyst powders (Mg–Al–SP, Cu–Mg–Al–SP, Cu–Mg–Al–SF, and Cu–Mg–Al–SF–SP) for each was placed in the middle section of the reactor. A reacting gas mixture containing 1 mL min^{-1} of O_2, 1 mL min^{-1} of CO, and 98 mL min^{-1} of N_2 was passed through the catalyst

bed at atmospheric pressure. All gas flows were controlled by mass flow controllers, which were calibrated by a soap bubble meter before test. The outlet gas composition was analyzed online using an Agilent 7890B gas chromatograph equipped with a packed column (Porapak N molSieve 5A) and a thermal conductivity detector (TCD).

3 Results and discussion

Figure 1 presents the small-angle XRD patterns of samples with different metals calcined at different temperatures. The sample Mg–Al-400 presented a strong (100) peak around 0.7° together with a weak (110) peak around 1.5°, indicating that the hexagonal ordered mesoporous structure was formed in the sample Mg–Al-400. Similarly, an obvious (100) and a weak (110) diffraction peaks were also detected in the sample Cu–Mg–Al-400, implying that the introduction of copper did not destroy the mesoporous structure. The good mesoscopic order was preserved even after calcining at 800 °C in the sample Cu–Mg–Al–SP, showing a good thermal stability of the mesoporous structure. The obtained long-range ordered mesopores could be further observed in the TEM images. As shown in Fig. 2a and b, the typical well-ordered hexagonal mesoporous structure was observed along the (110) direction in the samples Mg–Al-400 and Cu–Mg–Al–SP. It was also found that the incorporation of Cu into Mg–Al oxide via the one-pot method did not change the ordered mesoporous structure of Cu–Mg–Al–SP sample, and no additional isolated copper-based particle was observed over the entire network, as shown in Fig. 2b.

Wide-angle XRD patterns of Mg–Al–SP and Cu–Mg–Al–SP samples calcined at 800 °C are displayed in Fig. 3. Reflections of Mg–Al spinel phase (JCPDS No. 1-1157) at $2\theta = 19.1°$, 31.6°, 37.3°, 45.3°, 60.0°, and 66.2° were

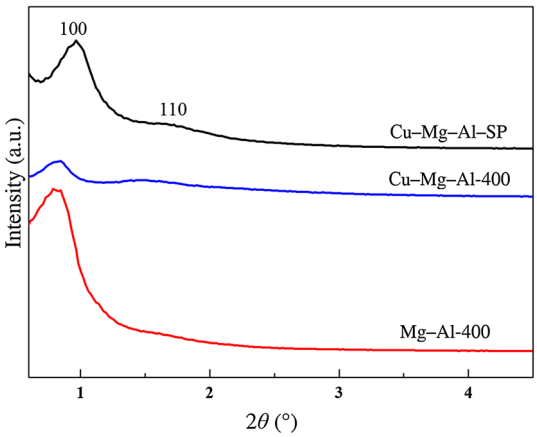

Fig. 1 (Color online) Small-angle XRD patterns of as-prepared Mg–Al-400, Cu–Mg–Al-400, and Cu–Mg–Al–SP

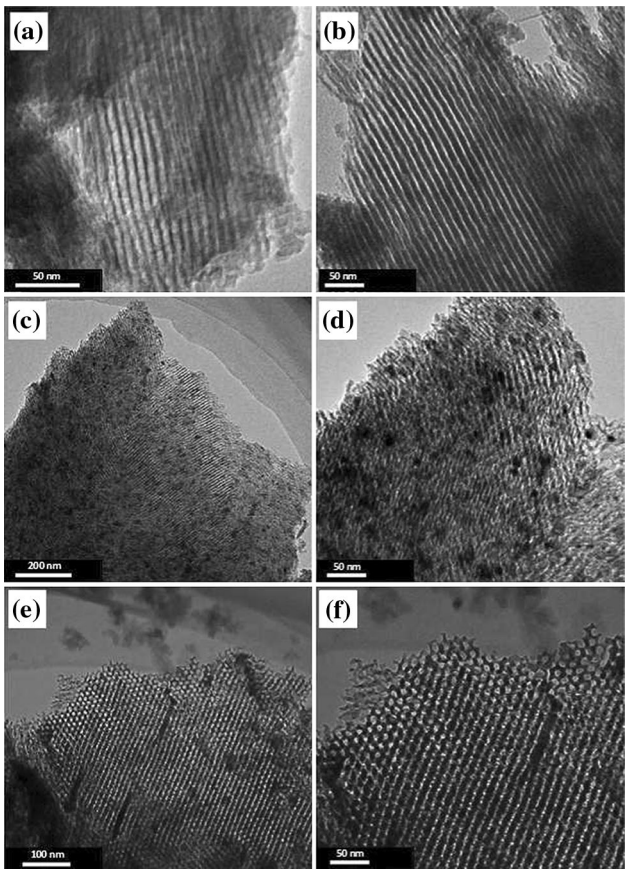

Fig. 2 TEM images of Mg–Al-400 (**a**), Cu–Mg–Al–SP (**b**), Cu–Mg–Al–SF (**c**, **d**), and Cu–Mg–Al–SF–SP (**e**, **f**)

verified, as shown in Fig. 3a. In the case of Cu–Mg–Al–SP (Fig. 3b), the calcination at 800 °C resulted in the phase composition similar to that observed in Mg–Al–SP sample. It is noteworthy that no XRD signal of metallic copper or copper oxide was detected. Compared with the cell parameter a ($a = b = c = 7.984$ Å) of spinel phase in the Cu-free Mg–Al–SP sample, the corresponding value ($a = b = c = 8.006$ Å) in Cu–Mg–Al–SP got larger. This probably attributed to the incorporation of larger Cu ions (0.73 Å) into the spinel lattice by replacing smaller Al^{3+} (0.53 Å), thus leading to a homogeneous distribution of copper on the atomic level in the Mg–Al spinel matrix, in accordance with the TEM image in Fig. 2b.

To investigate the structure properties of the obtained mesoporous composites, Cu–Mg–Al–SP sample was treated under different conditions in this work. Figure 3c shows the XRD pattern of Cu–Mg–Al–SF, which was derived from the pre-reduction of Cu–Mg–Al–SP sample under 5 vol% H_2 flow at 650 °C for 4 h. It can be seen that the spinel reflections were still retained, indicating the excellent stability of Mg–Al spinel matrix under reduction condition. In addition, the reflections at 43.3° and 50.4° are observed in Fig. 3c, indicating the formation of metallic

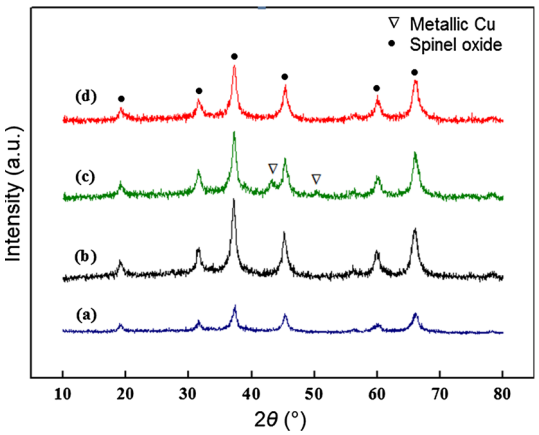

Fig. 3 (Color online) Wide-angle XRD patterns of Mg–Al–SP (**a**), Cu–Mg–Al–SP (**b**), Cu–Mg–Al–SF (**c**), and Cu–Mg–Al–SF–SP (**d**)

copper. Under H_2 atmosphere, the surface reduction of copper will lead to the continuous migration of copper ion from the bulk phase to the surface of spinel, which was followed by the reduction of copper ion on the inner/outer surface of the mesoporous composite. The continuous migration and reduction of copper ion at high temperature under H_2 atmosphere will lead to the formation of metallic copper particles in the composite system.

The morphology change of the sample upon H_2 reduction was further supported by TEM results. It can be seen from Fig. 2c, d, after reduction, the Cu nanoparticles (dark spots) with the size of 6–10 nm were uniformly dispersed over the ordered mesoporous network. In addition, the ordered mesoporous skeleton corresponding to the Mg–Al spinel was still maintained after the reduction. The textural stability of Cu–Mg–Al sample is also supported by nitrogen adsorption measurements. As shown in Fig. 4, both the nitrogen adsorption–desorption isotherms are type IV with H1 hysteresis loops in Cu–Mg–Al–SP and Cu–Mg–Al–SF samples, which indicated that the uniformity of the mesopores was still preserved after 4 h reduction at 650 °C. Furthermore, comparing to the as-synthesized Cu–Mg–Al–SP (S_{BET} = 137 m^2 g^{-1}), the specific surface area of the as-reduced sample slightly increased to 145 m^2 g^{-1}, further demonstrating the excellent stability of the mesoporous network.

Cu-based materials have been extensively considered as promising catalysts for CO oxidation [26–30]. As discussed above, copper existed either as lattice Cu ions on the atomic level in spinel phase or as nanoparticles distributed through the mesoporous Mg–Al spinel network. To correlate the structure property of catalyst with the catalytic performance, four different catalysts toward CO oxidation were tested in a fixed-bed reactor. Figure 5 depicts the profiles of CO conversion at different operation temperatures over Mg–Al–SP, Cu–Mg–Al–SP, Cu–Mg–Al–SF, and Cu–Mg–Al–SF–SP samples. In the absence of Cu, the Mg–Al–SP was almost catalytically inactive toward CO oxidation in the investigated temperature range. After Cu was incorporated into the Mg–Al spinel structure, forming spinel Cu–Mg–Al–SP, the activity was enhanced significantly. The Cu–Mg–Al–SP spinel was already active (13 %) even at 25 °C, and the CO conversion increased with the reaction temperature and reached 100 % at 270 °C, indicating that the copper existed in spinel phase was active for CO oxidation.

As discussed above, the pre-treatment of Cu–Mg–Al–SP spinel under hydrogen atmosphere led to the surface enrichment of copper, and the copper existed as small particles distributed through the mesoporous network. It is noted that metallic particles will be re-oxidized to copper oxide because excessive oxygen was fed during CO oxidation. It can be seen from Fig. 5 that the activity of Cu–Mg–Al–SF was significantly increased. For example, the CO conversion at 150 °C was enhanced from 14 % (for Cu–Mg–Al–SP) to 61 %, and the reaction temperature for

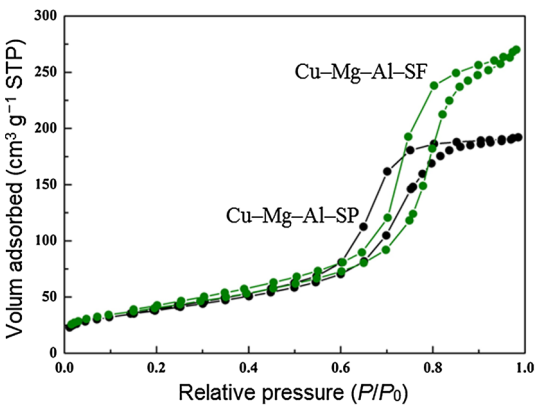

Fig. 4 (Color online) Nitrogen adsorption isotherms for Cu–Mg–Al–SP and Cu–Mg–Al–SF

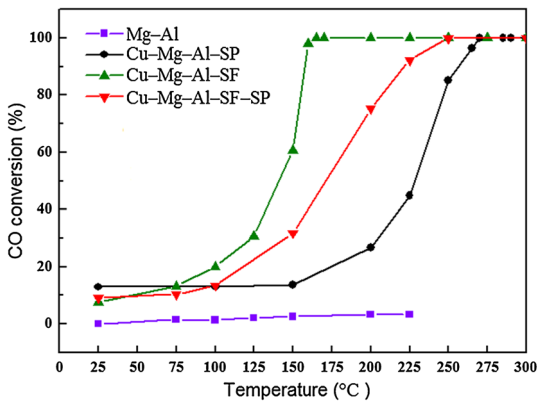

Fig. 5 (Color online) CO conversion as a function of reaction temperature over Mg–Al–SP, Cu–Mg–Al–SP, Cu–Mg–Al–SF, and Cu–Mg–Al–SF–SP

complete oxidation of CO was lowered by 105 °C, indicating that the copper existed as nanoparticles on the Mg–Al spinel surface is much more active than that existed as lattice Cu ions in spinel phase.

In addition, the spent catalyst Cu–Mg–Al–SF was further treated at 650 °C for 1 h under the reaction gas feed (O_2/CO/N_2 = 1:1:98), and the resulted sample was denoted as Cu–Mg–Al–SF–SP. It can be seen from Fig. 5 that the activity of the Cu–Mg–Al–SF–SP is higher than that of the Cu–Mg–Al–SP and lower than that of Cu–Mg–Al–SF. This moderate catalytic performance might be related to the state of copper in the mesoporous composite catalyst. Thus, XRD was used to analyze the phase composition of Cu–Mg–Al–SF–SP. It can be seen from Fig. 3 that XRD patterns of the sample Cu–Mg–Al–SF–SP were very similar to those of the as-synthesized Cu–Mg–Al–SP sample, and no other copper-based phase was detected in Cu–Mg–Al–SF–SP, indicating that the re-incorporation of copper into the mesoporous spinel network took place after treating the sample under oxygen-containing gas mixture at higher temperature. This can be further confirmed by the TEM images in Fig. 2e, f. The migration of copper from the surface to bulk spinel phase led to the decrease in the catalytic activity toward CO oxidation, which further supports the above conclusion that copper existed as nanoparticles on the Mg–Al spinel surface is much more active than that existed as lattice Cu ions in spinel phase.

The state of copper in the mesoporous composite catalysts was further supplemented by the TPR results. Figure 6 presents the reduction profiles of Cu–Mg–Al–SP, Cu–Mg–Al–SF, and Cu–Mg–Al–SF–SP. For the as-synthesized Cu–Mg–Al–SP, a broad reduction peak centered at around 305 °C was observed, which can be assigned to the reduction of copper ion in bulk spinel phase [31–33]. After H_2 treatment, according to the above discussion, copper existed as metallic nanoparticles that well decorated the mesoporous skeleton, followed by the re-oxidation and formation of CuO nanoparticles on the surface when exposed to oxygen. Accordingly, the reduction behavior of Cu–Mg–Al–SF is similar to that of copper oxide nanoparticles, and the reduction peak shifted toward low temperature, centering at 220 °C [34, 35]. Interestingly, after treating the spent Cu–Mg–Al–SF at 650 °C for 1 h in the presence of oxygen-containing gas mixture, the reduction peak of the resulted sample Cu–Mg–Al–SF–SP shifted to higher temperature (Fig. 6), indicating the re-incorporation of copper into spinel phase. It is noted that the reduction temperature of Cu–Mg–Al–SF–SP centered at around 290 °C is higher than that of Cu–Mg–Al–SF and lower than that of Cu–Mg–Al–SP, which is in accordance with their catalytic performance.

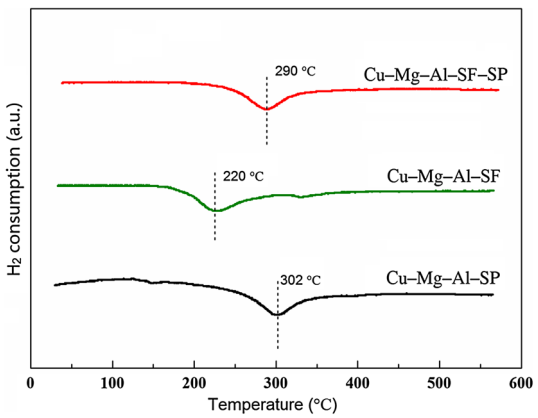

Fig. 6 (Color online) TPR profiles of Cu–Mg–Al–SP, Cu–Mg–Al–SF, and Cu–Mg–Al–SF–SP

4 Conclusions

In summary, the effect of reduction–oxidation treatment on structure and catalytic properties of ordered mesoporous Cu–Mg–Al composite oxides was studied in this work. Using a simple one-pot evaporation-induced self-assembly process followed by further thermal treatment, copper was first homogeneously incorporated into the mesoporous spinel matrix. After a reduction–oxidation treatment, copper migrated from bulk spinel phase to the surface. In the resulted mesoporous composite, copper presented as nanoparticles that well decorated the parent mesoporous skeleton composed of Mg–Al spinel. In addition, the Cu-incorporated Mg–Al spinel structure could be retrieved after thermal treatment of the sample under oxidic atmosphere at a higher temperature. By the comparative analysis of catalytic performance based on different catalysts, it was found that copper existed as nanoparticles on the surface of mesoporous Mg–Al skeleton is much more active toward CO oxidation than that presented as lattice Cu ions in spinel phase.

Acknowledgments This work was supported by the Recruitment Program of Global Youth Experts of China, the National Natural Science Foundation of China (21403267, 21450110410), and Shandong Postdoctoral Innovation Program (201303065).

Conflict of interest The authors declare that they have no conflict of interest.

References

1. Gamarra D, Belver C, Fernández-García M et al (2007) A selective CO oxidation in excess H_2 over copper-ceria catalysts: identification of active entities/species. J Am Chem Soc 129:12064–12065

2. Jiang HQ, Cao ZW, Schirrmeister S et al (2010) A coupling strategy to produce hydrogen and ethylene in a membrane reactor. Angew Chem Int Ed 49:5656–5660
3. Jiang HQ, Wang HH, Liang FY et al (2009) Direct decomposition of nitrous oxide to nitrogen by in situ oxygen removal with a perovskite membrane. Angew Chem Int Ed 48:2983–2986
4. Remediakis IN, Lopez N, Nørskov JK (2005) CO oxidation on rutile-supported Au nanoparticles. Angew Chem Int Ed 44:1824–1826
5. Zhu YY, Wang XD, Huang YQ et al (2012) Identification of the crystallographic sites of Ir in $BaIr_{0.2}FeAl_{10.8}O_{19}$ hexaaluminate. J Phys Chem C 116:24487–24495
6. Zhang Y, Wang XD, Zhu YY et al (2013) Stabilization mechanism and crystallographic sites of Ru in Fe-promoted barium hexaaluminate under high-temperature condition for N_2O decomposition. Appl Catal B 129:382–393
7. Burch R (1996) Low NO_x options in catalytic combustion and emission control. Pure Appl Chem 68:377–385
8. Burch R (1997) Low NO_x options in catalytic combustion and emission control. Catal Today 35:27–36
9. Qian JC, Chen ZG, Liu CB et al (2014) Biotemplated fabrication of hierarchical mesoporous CeO_2 derived from diatom and its application for catalytic oxidation of CO. Chin Sci Bull 59:3260–3265
10. Zhang WD, Lu XF, Zhou WL et al (2014) Mesoporous iron oxide-silica supported gold catalysts for low-temperature CO oxidation. Chin Sci Bull 59:4008–4013
11. Gu D, Schüth F (2014) Synthesis of non-siliceous mesoporous oxides. Chem Soc Rev 43:313–344
12. Zhao DY, Huo QS, Feng JL et al (1998) Nonionic triblock and star diblock copolymer and oligomeric surfactant syntheses of highly ordered, hydrothermally stable, mesoporous silica structures. J Am Chem Soc 120:6024–6036
13. Fukuoka A, Araki H, Kimura JI et al (2004) Template synthesis of nanoparticle arrays of gold, platinum and palladium in mesoporous silica films and powders. J Mater Chem 14:752–756
14. Li L, Shi JL, Yan JN (2004) A highly efficient heterogeneous catalytic system for heck reactions with a palladium colloid layer reduced in situ in the channel of mesoporous silica materials. Chem Commun 17:1990–1991
15. Zhao RH, Li CP, Guo F et al (2007) Scale-up preparation of organized mesoporous alumina in a rotating packed bed. Ind Eng Chem Res 46:3317–3320
16. Wu ZX, Li Q, Feng D et al (2010) Ordered mesoporous crystalline γ-Al_2O_3 with variable architecture and porosity from a single hard template. J Am Chem Soc 132:12042–12050
17. Huo QS, Margolese DI, Ciesla U et al (1994) Generalized synthesis of periodic surfactant/inorganic composite materials. Nature 368:317–321
18. Bai P, Wu PP, Yan ZF et al (2009) Cation-anion double hydrolysis derived mesoporous γ-Al_2O_3 as an environmentally friendly and efficient aldol reaction catalyst. J Mater Chem 19:1554–1563
19. Yuan Q, Yin AX, Luo C et al (2008) Facile synthesis for ordered mesoporous γ-aluminas with high thermal stability. J Am Chem Soc 130:3465–3472
20. Morris SM, Fulvio PF, Jaroniec M (2008) Ordered mesoporous alumina-supported metal oxides. J Am Chem Soc 130:15210–15216
21. Yuan Q, Duan HH, Li LL et al (2010) Homogeneously dispersed ceria nanocatalyst stabilized with ordered mesoporous alumina. Adv Mater 22:1475–1478
22. Cai WK, Yu J, Anand C et al (2011) Facile synthesis of ordered mesoporous alumina and alumina-supported metal oxides with tailored adsorption and framework properties. Chem Mater 23:1147–1157
23. Jiang HQ, Bongard H, Schmidt W et al (2012) One-pot synthesis of mesoporous Cu-γ-Al_2O_3 as bifunctional catalyst for direct dimethyl ether synthesis. Microporous Mesoporous Mater 164:3–8
24. Sun LB, Tian WH, Liu XQ (2009) Magnesia-incorporated mesoporous alumina with crystalline frameworks: a solid strong base derived from direct synthesis. J Phys Chem C 113:19172–19178
25. Wang N, Shen K, Huang LH et al (2013) Facile route for synthesizing ordered mesoporous Ni-Ce-Al oxide materials and their catalytic performance for methane dry reforming to hydrogen and syngas. ACS Catal 3:1638–1651
26. Gu D, Jia CJ, Bongard H et al (2014) Ordered mesoporous Cu–Ce–O catalysts for CO preferential oxidation in H_2-rich gases: influence of copper content and pretreatment conditions. Appl Catal B 152:11–18
27. Yang BL, Chan SF, Chang WS et al (1991) Surface enrichment in mixed oxides of Cu, Co and Mn, and its effect on CO oxidation. J Catal 130:52–61
28. Liu W, Flytzanistephanopoulos M (1995) Total oxidation of carbon monoxide and methane over transition metal fluorite oxide composite catalysts: I. Catalyst composition and activity. J Catal 153:304–316
29. Liu W, Flytzanistephanopoulos M (1995) Total oxidation of carbon-monoxide and methane over transition metal fluorite oxide composite catalysts: II. Catalyst characterization and reaction-kinetics. J Catal 153:317–332
30. Avgouropoulos G, Ioannides T (2003) Selective CO oxidation over CuO–CeO_2 catalysts prepared via the urea-nitrate combustion method. Appl Catal A 244:155–167
31. Kawabata T, Matsuoka H, Shishido T et al (2006) Steam reforming of dimethyl ether over ZSM-5 coupled with Cu/ZnO/Al_2O_3 catalyst prepared by homogeneous precipitation. Appl Catal A 308:82–90
32. Xing Y, Liu ZX, Suib SL (2007) Inorganic synthesis for the stabilization of nanoparticles: application to Cu/Al_2O_3 nanocomposite materials. Chem Mater 19:4820–4826
33. Behrens M, Kasatkin I, Kuhl S et al (2010) Phase-pure Cu, Zn, Al hydrotalcite-like materials as precursors for copper rich Cu/ZnO/Al_2O_3 catalysts. Chem Mater 22:386–397
34. Luo MF, Zhong YJ, Yuan XX et al (1997) TPR and TPD studies of CuO/CeO_2 catalysts for low temperature CO oxidation. Appl Catal A 162:121–131
35. Luo MF, Zheng XM (1998) Redox behaviour of CeO_2 and $Ce_{0.5}Zr_{0.5}O_2$ supported CuO catalysts for CO oxidation. Acta Chem Scand 52:1183–1187